Discover Mechanical Engineering

Research

Mechanical model for the compression of weft-knitted spacer fabrics

Ulysse Le Coz[1] · Yue Zhang[1] · Pierre Ringenbach[1] · Atsushi Sakuma[1] · Annie Yu[2]

Received: 7 November 2024 / Accepted: 25 April 2025
Published online: 22 May 2025

Abstract
Weft-knitted spacer fabrics are thick 3D knitted structures notable for their cushioning properties, until now their mechanical behaviour was almost only empirically compiled without being understood nor directly linked to the fabric's properties. The current effort to describe the fabrics geometry focuses on extremely complex models when a mechanical model requires a simple one. This study investigated 4 different weft-knitted spacer layer geometries through FEA simulations, it identified the model composed of two arcs bending in opposite directions to match very well the compression behaviour of the samples. The Euler buckling load and Euler–Bernoulli beam theory were successfully used with the selected geometrical model to predict the plateau force (average error 22.7%, $R^2 = 0.91$) and the Young's modulus (average error 38.7%, $R^2 = 0.66$) of the experimental samples. The study also investigated a compression behaviour model describing the compression of weft-knitted spacer fabrics until the plateau phase, giving predictions based on the fabric's structure and materials showing a $35.8 \pm 18.2\%$ average error. A simple geometrical model was also developed to predict the buckling thickness of the spacer layer (average error of 15.9%, $R^2 = 0.85$). Those finding can trigger a great acceleration of research on spacer fabrics by reducing the important time allowed to empirical samples production and testing and open a path of selected production helped using formulas and solvers.

Keywords Weft knitted spacer fabrics · Mechanical model · FEA · Simulation · Compression · Beam theory

List of symbols

A_{loop}	Average area of the outer layer's loops
A_{platen}	Area of the compression platen
A_{unit}	Average compression area of the spacer units
C_{mod}	Error coefficient of the model prediction
C_s	Error coefficient of the invert analysis
C_{sim}	Error coefficient of the simulation results
E	Effective Young's modulus in compression of the fabric in the thickness direction
e	Effective compression stiffness of the fabric in the thickness direction
e'	Compression stiffness of the spacer units in the thickness direction
F	Compression force of the fabric in the thickness direction
F'	Compression force of the standard spacer unit in the thickness direction
F_b	Buckling force of the spacer unit
F_b'	Buckling force of the standard unit
F_{bu}	Buckling force of the unit u

✉ Ulysse Le Coz, ulysse.lecoz@yahoo.fr | [1]Department of Advanced Fibro-Science, Kyoto Institute of Technology, Sakyo-ku, Kyoto, Japan. [2]School of Fashion and Textiles, The Hong Kong Polytechnic University, Hong Kong, China.

F_p Plateau force of the spacer fabric
F_p' Plateau force of the standard unit
F_{pu} Plateau force of the unit u
F_{nb} Model compression force of the fabric neglecting the buckling
F_0 Compression force at the start of the standard analysis
G Distance between the needles on the knitting machine needle bed
H Height of the outer layer's loop
I_b Irregularity of the of the fabric buckling force normal distribution
L Length of the spacer yarn between the tucks
n Needle distance between the tucks
N_u Number of spacer units under the compression platen
S_t Standard deviation of the thickness normal distribution
S_b Standard deviation of the fabric buckling force normal distribution
S_b' Standard deviation of the spacer units buckling force normal distribution
W Width of the outer layer's loops
T Distance between the compression platen and the support during the compression
T' Spacer layer thickness
T_{av} Average thickness of the fabric
T_{av}' Average thickness of the spacer layer
T_b Buckling thickness of the spacer fabric
T_b' Buckling thickness of the standard unit
T_{bu} Buckling thickness of the unit u
T_i Ideal thickness of the spacer layer
T_k Thickness of the spacer layer on the knitting machine
T_m Model thickness of the spacer layer
T_{out} Thickness of the outer layer's surface covering the spacer layer
T_0 Thickness of the fabric at the start of the standard analysis
u Spacer unit
δ Displacement of the compression platen
δ_{av} Displacement at the average thickness of the fabric
δ_b Displacement at the buckling thickness of the standard unit
δ_c Displacement at the initial contact between the platen and the fabric
δ_{max} Initial distance between the compression platen and the support
δ_0 Displacement at the start of the standard analysis
ε Compression strain of the fabric in the thickness direction
ε_p Compression strain of the fabric at the beginning plateau phase
f_t Probability density function of the fabric thickness distribution
f_t' Probability density function of the spacer layer thickness distribution
Φ_t Cumulative distribution function of the fabric thickness distribution
f_b Probability density function of the buckling force distribution
Φ_b Cumulative distribution function of the buckling force distribution
σ Compression stress of the fabric in the thickness direction
σ_p Compression stress of the fabric at the beginning of the plateau phase

1 Introduction

Weft-knitted spacer fabrics are 3D knitted structures with a high thickness and spring-like compression properties [1]. Despite their geometrical structure and their compression behaviour being their main interest, neither of them can be predicted before knitting the fabrics. This study investigates 4 different geometrical models based on the knitting machine and spacer fabrics' geometrical properties and identifies the most suitable using a FEA. The study then proposes a mechanical model to predict the stiffness, the thickness, the plateau force and the plateau strain of weft-knitted spacer fabrics.

Spacer fabrics can serve a variety of purposes [2–10], but they are mostly used for their cushioning [11–22] properties. Their compression behaviour was quite studied, but only in an empirical way [11–16, 23–26].

A compression behaviour model needs to be based on a geometrical model first. A geometrical model developed by Wu and Xia was tested with success using FEA, but the model is complex and cannot predict a compression behaviour without simulations, thus it was tested on only one sample [27]. In this study, simulations are conducted using simple geometrical models suitable for a simple mechanical model which could be later used without conducting any simulation.

Several mechanical models have already been proposed to describe the compression behaviour of spacer fabrics, but they could not explain nor predict the behaviour of the fabrics [28–30]. In a previous study a model decomposing the spacer fabric as a set of springs whose characteristics followed a normal distribution was developed to describe the flattening behaviour of weft-knitted spacer fabrics [31]. This model is now combined with the Euler–Bernoulli beam theory to presents a complete compression behaviour model expressing the compression force of a weft-knitted spacer fabric in function of its structure and material properties.

This study is pursuing two aims: providing a relevant geometrical model for the spacer layer and a mechanical model predicting accurately the compression behaviour of the fabric. The achievement of these two aims is to be validated by the match between the properties obtain through the simulations, the properties measured on experimental samples and the properties predicted by the mechanical model.

2 Materials and methods

2.1 Materials

A spacer fabric is a three layers sandwich material: its two outer layers are parallel flat fabrics connected by spacer yarns. The weft-knitted spacer fabrics investigated in this study have plain knitted outer layers and spacer yarns connecting them by successively tucking them following the weft direction (Fig. 1). The spacer yarn never knits and only tucks and floats, the floats of the spacer yarns create a spacer layer between the outer layers (Fig. 2).

The samples were produced on a 10-gauge double-bed weft-knitting machine of the grade "SWG 091N2" (Shima Seiki MFG. LTD.; Wakayama, Japan); the machine has a needle gap $G = 2.54$ mm, a knitting thickness $T_k = 3.5$ mm and knitting needles with a circular section of radius $R_n = 0.6$ mm. The yarns properties are listed in Table 1 and are presented with more details in the weft-knitted spacer flattening study [31]. The experimental samples are listed in the Table 2, they were all knitted with 70 and 0 stitch values for the outer layer and the spacer layer respectively except for the spacer yarn of the A12N3T S10 sample which has a stitch value of 10.

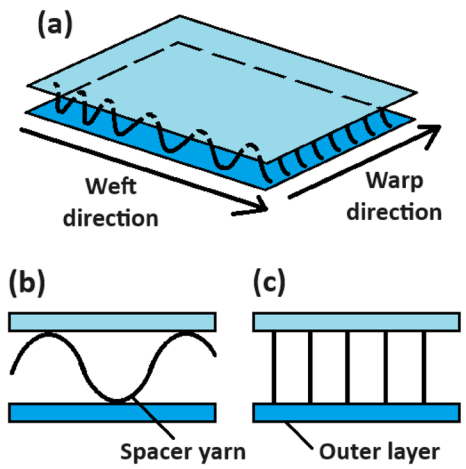

Fig. 1 (**a**) Isometric view, (**b**) warp view and (**c**) weft view of a weft-knitted spacer fabric

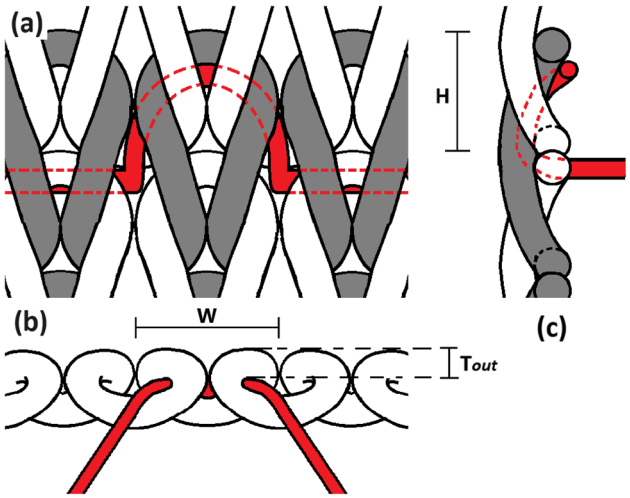

Fig. 2 A spacer yarn (red) tucking the outer layer (white and grey) in (**a**) top view, (**b**) warp view and (**c**) weft view

Table 1 Yarns properties

Commercial name	Function	Material	Diameter (mm)	Linear density (Tex)	Stiffness for a 100mm yarn (cN/mm)	Tenacity (cN/Tex)
Amossa LS1/20	Outer layer yarn	PET	/	50	29.70 ± 7.4	39.86 ± 0.62
Dralon-Cotton Ne32/1		Cotton 50% -acrylic 50%			47.97 ± 18.2	13.23 ± 1.01
Marulon ST6800	Elastic yarn	Spandex	/	39	0.49 ± 0.06	6.58 ± 0.99
Marulon S1470				15	0.15 ± 0.02	10.52 ± 1.97
	Spacer yarn(monofilament)	Polyamide 6	0.08	5.4	17.60 ± 5.54	/
			0.12	12.3	38.59 ± 4.75	
/			0.14	16.7	51.01 ± 5.67	
		PET	0.08	6.9	41.58 ± 6.18	

2.2 Geometrical models

The knitting structure of a weft-knitted spacer fabric is defined by its needle distance *n*, which represents the number of needles horizontally separating two following tucks. For a stable knitting, each loop of the outer layer can accommodate only one tuck of the spacer yarn (Fig. 2), 2*n* different spacer yarns are required to tuck all the loops on a same row of the outer layer. During the knitting process the spacer yarn is straight between the tucks on the flat-knitting machine, its length *L* between two following tucks is calculated using the Eq. 1. When the knitting is over the spacer fabric falls from the machine, the outer layer which is no longer held by the knitting needles shrinks until its loops reach an average width *W* (Fig. 2).

$$L = \sqrt{T_k{}^2 + (n \times G)^2} \tag{1}$$

By considering that the spacer yarn remains straight during and after the shrinkage, the ideal thickness T_i of the spacer layer can be calculated using the Eq. 2. Despite ignoring T_{out} the thickness of the outer layer covering the spacer layer, this formula has already shown good predictions of the fabric thickness [1]. The geometry of the spacer layer between two following tucks is called a spacer unit. Because the total geometry of the spacer layer is the repetition in both the warp and weft directions of the spacer unit, a geometrical model of the spacer unit is sufficient to describe the geometry of the whole spacer layer.

$$T_i = \sqrt{L^2 - (n \times W)^2} \tag{2}$$

Table 2 Weft-knitted spacer fabric samples properties

Outer layer Yarn material	Spacer yarn material	Spacer yarn diameter (mm)	Needle distance	Elastic yarn	Samplename
Cotton-acrylic	Polyamide 6	0.12	5	39Tex yarn	DA12N5L
			7		DA12N7L
PET		0.08	5		A8N5L
		0.12			A12N5L
		0.14			A14N5L
		0.08	7		A8N7L
		0.12			A12N7L
		0.14			A14N7L
		0.08	3	15Tex yarn	A8N3T
		0.12			A12N3T
		0.12			A12N3T S10
		0.14			A14N3T
		0.08	5		A8N5T
		0.12			A12N5T
		0.14			A14N5T
		0.08	7		A8N7T
		0.12			A12N7T
		0.14			A14N7T
	PET	0.08	3		E8N3T
			5		E8N5T

In this article, 4 geometrical models of spacer layer are investigated:

The direct model (Fig. 3a) considers the spacer yarn to keep its shape after the knitting needles caught the spacer yarn on the machine. It is composed of a long straight line with two small arcs of radius R_n at is extremities. Those arcs are tangent to both the horizontal outer layer and to the straight long line. This model being very similar to the ideal geometry of the spacer layer, its thickness is considered to be T_i.

The S-shaped model (Fig. 3b) assumes the spacer yarn to form an arc of width G to get out of a tuck and keeps its shape during and after the shrinkage. The two arcs are tangent to both the horizontal outer layers and to a straight long line connecting them. The model thickness is approximated to T_i.

The curved model (Fig. 3c) is based on the hypothesis that the spacer yarn initially forms arcs of width G to get out of the tucks on both outer layers, but that during the shrinkage the spacer yarn extremities are pushed toward one another contracting one arc into an arc of width W (Fig. 2) and bending the line in the middle. The three arcs are tangent to each other and to the horizontal outer layers. The model thickness is approximated to T_i.

The arc model (Fig. 3d) considers that the spacer layer is composed of two equal arcs of angle 2α and radius R_m, the arcs are tangent to each other and to the outer layers. The spacer yarn has totally lost the straight shape it had on the

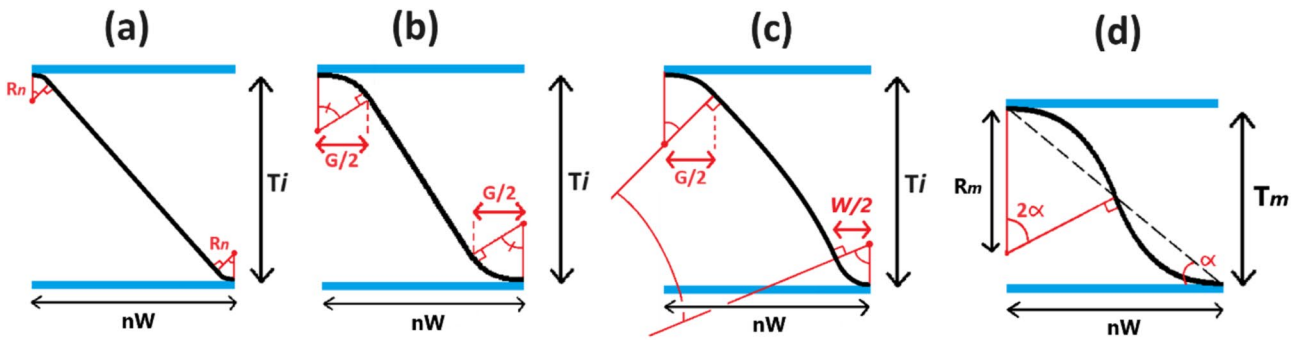

Fig. 3 (**a**) Direct model; (**b**) S-shaped model; (**c**) curved model; (**d**) arc model

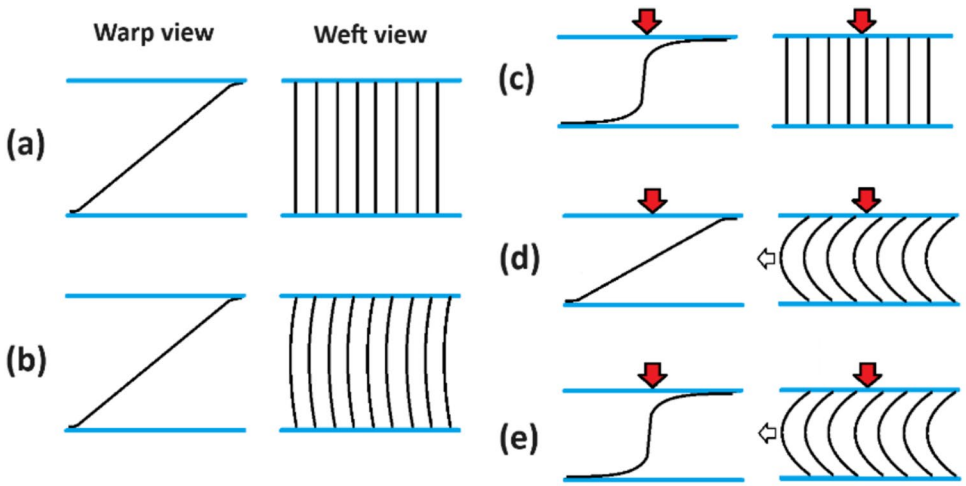

Fig. 4 (**a**) Straight model; (**b**) bent model; (**c**) model bending only within the plan during the compression; (**d**) model bending only out of the plan during the compression; (**e**) model bending within and out of the plan during the compression

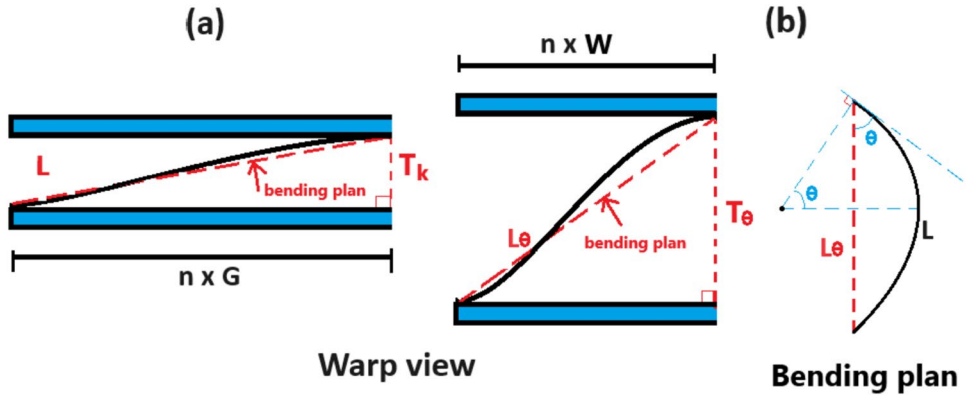

Fig. 5 Geometry of the bent model (**a**) on the machine and (**b**) after the shrinkage

knitting machine; to keep the spacer yarn length equal to L the model cannot have a thickness T_i. The arc model has a model thickness T_m given by the Eqs. 3 and 4.

$$2\alpha = \sqrt{10 - 2\sqrt{30\frac{n \times W}{L} - 5}} \tag{3}$$

$$T_m = \mathrm{n} \times \mathrm{W} \times \tan\alpha \tag{4}$$

A spacer layer geometrical model can be straight (Fig. 4a) with the spacer yarn going from one tuck to the other while remaining within a plan normal to the warp direction. A model could also be bent (Fig. 4b) with the spacer yarn going from one tuck to the other following a 3D trajectory projecting an arc on the plan normal to the weft direction. The straight models can show three different compression behaviours: the spacer yarn can bend only within the plan normal to the warp direction (Fig. 4c), it can buckle at the beginning of the compression and then bend out of the plan (Fig. 4d), or it can start to bend within the plan to then buckle and bend in the warp direction (Fig. 4e). The bent models cannot bend only within the plan and don't need to buckle to bend in the warp direction. If the geometry of the spacer yarn in the plan provides too much resistance the spacer unit will tend to bend mostly in the warp direction (Fig. 4d), if not the spacer yarn will bend in both ways (Fig. 4e).

The geometry of the bent models can be determined considering that the spacer yarn bends within a bending plan generated by both the warp direction and the direct line between the two tucks (Fig. 5a). The spacer yarn bends as a perfect arc within the bending plan, keeping its total length L. For an initial bending angle Θ, the distance between two tucks in the plan normal to the warp direction becomes L_Θ and the thickness becomes $T\Theta$ (Eqs. 5 and 6) (Fig. 5b).

$$L_\theta = L \times \frac{\sin\theta}{\theta} \tag{5}$$

$$T_\theta = \sqrt{{L_\theta}^2 - (n \times W)^2} \tag{6}$$

2.3 Simulation conditions

The geometry of a spacer unit strongly depends on the loop width W which can only be known from the measurement of the outer layer's weft density after its shrinkage. Because the fabric shrinkage cannot be simulated, model dimensions for the loops of the outer layer are used. The simplified geometrical model of a weft knitted loop developed by Pierce [32] gives the model values for the average loop width $W = 4D_{out}$ and the loop height $H = 2\sqrt{3} \times D_{out}$ in function of the outer layer yarn's diameter D_{out} (Fig. 2). The model value of the diameter of a cotton yarn D_{cotton} (m) is calculated in function of its linear density λ(Tex) using the Eq. 7 [33]. The PET and cotton-acrylic yarns are considered to have a similar porosity and structure to the cotton yarns but different fibre densities. The cotton fibres have a density $d_{cotton} = 1.54$ g/cm^3 while the PET has a density $d_{pet} = 1.38$ g/cm^3. Because the acrylic has a density of 1.18 g/cm^3 the cotton-acrylic yarns are considered to have an average fibre density similar to d_{pet}. The two outer layer yarns having a linear density $\lambda = 50$Tex, the Eqs. 7 and 8 give the model value $D_{out} = 0.381$ mm for both yarns.

$$D_{cotton} = \left(-0.10284 + 1.592 \times \sqrt{\frac{\lambda}{590{,}5}}\right) \times 10^{-3} \tag{7}$$

$$D_{out} = D_{cotton} \times \sqrt{\frac{d_{cotton}}{d_{pet}}} \tag{8}$$

The simulation models were designed on *SolidWorks2020* by sweeping a circular section on the different spacer unit geometries. The models were then meshed on *Femap* using hexahedral parts with volumes of a scale 10^{-6}mm^3. The finite element analysis was conducted on *LS-Dyna* were the three parts of each model (the top layer, the spacer layer and the bottom layer) were connected by mortar contacts. The top surface of the top layer was subjected to a forced displacement of speed 0.1 mm s^{-1} in the thickness direction (on the y-axis) while the bottom surface of the bottom layer was fixed in the thickness direction. The lateral edges of the spacer units are symmetry plans, the surfaces on those edges were fixed in the warp and weft directions (respectively the x-axis and z-axis) to insure that during the compression the unit model is only deformed in the thickness direction (Fig. 6). The edge surfaces normal to the weft direction also had fixed rotations on every axis since within the fabric the spacer yarn is hold tightly in the tuck and cannot rotate. The spacer yarn material was

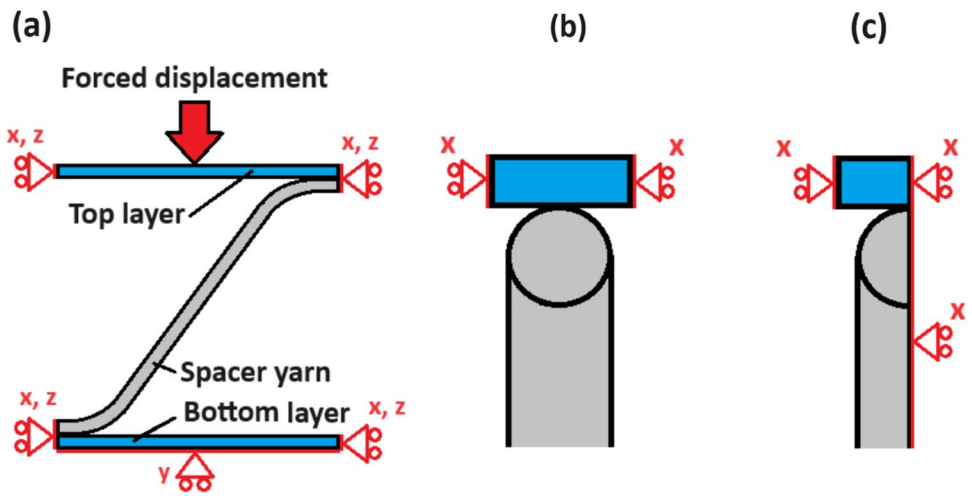

Fig. 6 Simulation conditions from the warp view (**a**), the weft view for straight-full (**b**) and half models (**c**)

Table 3 Simulation models of a A12N5 spacer unit

Spacer yarn material	Spacer yarn diameter	Needle distance *n*	Geometrical model	Simulation model	Simulation model name
Polyamide 6	0.12 mm	5	Direct	straight—half	A12N5-DH
				straight—full	A12N5-D
				$\Theta = 1^{\circ}$	A12N5-D1
				$\Theta = 5^{\circ}$	A12N5-D5
			S-shaped	straight—half	A12N5-SH
				straight—full	A12N5-S
				$\Theta = 1^{\circ}$	A12N5-S1
				$\Theta = 5^{\circ}$	A12N5-S5
			Curved	straight—half	A12N5-CH
				straight—full	A12N5-C
				$\Theta = 1^{\circ}$	A12N5-C1
				$\Theta = 5^{\circ}$	A12N5-C5
			Arc	straight—half	A12N5-AH
				straight—full	A12N5-A
				$\Theta = 1^{\circ}$	A12N5-A1
				$\Theta = 5^{\circ}$	A12N5-A5

Table 4 Simulation models of a spacer unit using the arc geometrical model

Spacer yarn material	Spacer yarn diameter (mm)	Needle distance	Simulation model name
PET	0.08	3	E8N3-A
Polyamide 6			A8N3-A
	0.12		A12N3-A
	0.14		A14N3-A
PET	0.08	5	E8N5-A
Polyamide 6			A8N5-A
	0.12		A12N5-A
	0.14		A14N5-A
	0.08	7	A8N7-A
	0.12		A12N7-A
	0.14		A14N7-A

considered isotropic, respective Young's modulus of 3.4 and 8.3GPa were used for the Polyamide 6 and the PET. The simulation neglected the friction due to the spacer yarn being tightly held in the outer layer tuck.

A first group of simulations was conducted with 16 different models of a spacer unit A12N5 of needle distance $n = 5$ and Polyamide 6 spacer yarn of diameter $D_{spacer} = 0.12$ mm, the simulation models are listed in the Table 3. Each of the 4 geometrical models (direct, S-shaped, curved and arc) was used to produce 4 simulations models: a straight full model, a straight half model, a bent model of initial angle $\Theta = 1^{\circ}$ and a bent model of initial angle $\Theta = 5^{\circ}$.

A second group of simulations was then conducted using only the straight full arc models listed in the Table 4, 11 different models of spacer unit of different needle distances *n*, spacer yarn materials and spacer yarn diameters D_{spacer} were used.

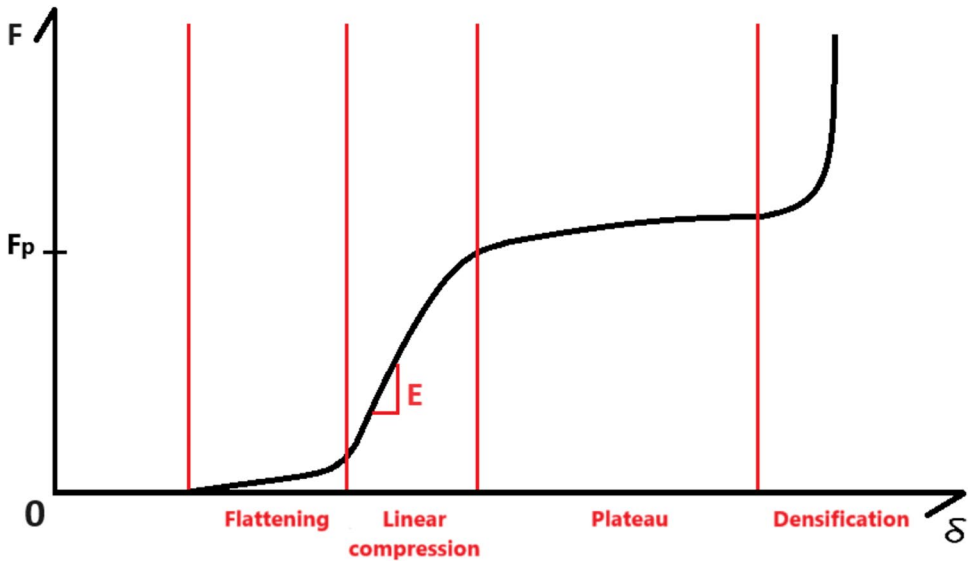

Fig. 7 Compression behaviour of the spacer fabrics

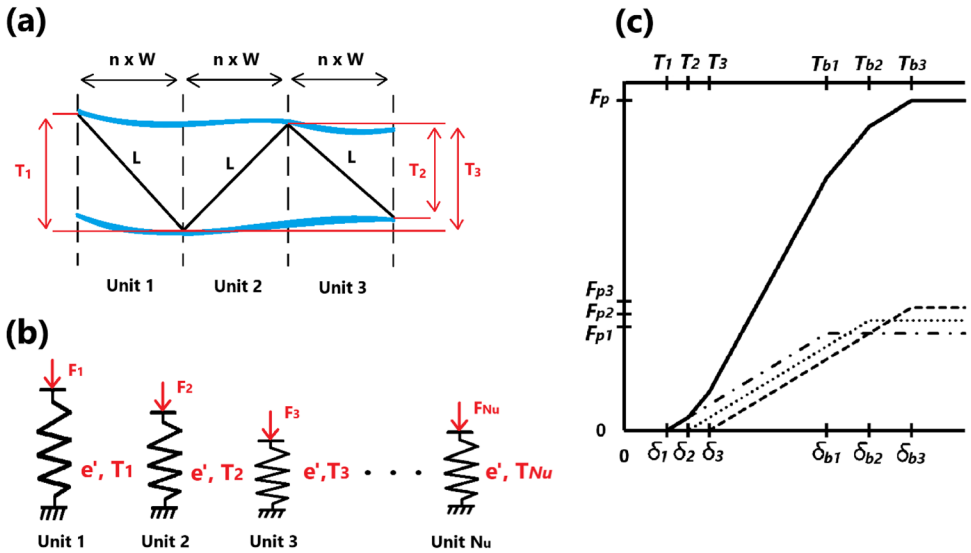

Fig. 8 Spacer units (**a**) geometry and (**b**) spring-like characteristics; (**c**) fabric compression behaviour

2.4 Mechanical model

2.4.1 Compression behaviour model

A spacer fabric compressed in its thickness direction between two flat compression platens initially at a distance δ_{max} shows a compression behaviour following four phases: the flattening, the linear compression, the plateau and the densification [11, 14, 31] (Fig. 7). The densification phase is caused by the compression of the outer layers afters the spacer layer has lost all its thickness; it is not investigated in this study.

The spacer units are considered to behave like independent springs with linear compression behaviours of a same stiffness e'. The outer layer does not participate to the spring-like compression behaviour; to describe this behaviour this study uses the spacer layer thickness $T' = T - 2T_{out}$. A spacer unit u has a thickness T_u and starts its linear compression at a displacement $\delta_u = \delta_{max} - T_u - 2T_{out}$. When the compression resistance F_u of the unit u reaches its buckling force F_{bu}, the spacer yarn buckles, and the force drops to a plateau force F_{pu} to remain constant. Each loop of the top outer layer being supported by two units (Figs. 2, 8a), the average compression area of the units A_{unit} is half the average loop area A_{loop}. The total compression force of a specimen is the sum of the compression forces F_u of all the N_u spacer units subjected to the compression (Eqs. 9, 10). Due to the diversity of unit thickness within the fabric the units do

not start their compression at the same time (Fig. 8a, b), the fabric starts to show a linear compression behaviour only when most of the units are being pressed (Fig. 8c). The units buckle one after the other, therefor the fabric compression reaches its plateau phase gradually. Because the difference of force between F_{bu} and F_{pu} can neither be predicted nor measured they are considered equal by this study.

$$N_u = \frac{A_{platen}}{A_{unit}} = \frac{2 \times A_{platen}}{A_{loop}} = \frac{2 \times A_{platen}}{W \times H} \tag{9}$$

$$F(\delta) = \sum_{u=1}^{u=N_u} F_u(\delta) \tag{10}$$

The spacer units pressed together during a compression test cannot be characterised directly, the characterisation of the fabric focus on the determination of a standard spacer unit. This standard unit is defined as average in all its characteristics: it has an average thickness T_{av}' (Eq. 11), an average buckling thickness T_b' (Eq. 12) and an average plateau force F_p' (Eq. 13). The standard unit compression force $F'(\delta)$ shows a linear behaviour from $\delta_{av} = \delta_{max} - T_{av}' - 2T_{out}$ and buckles at the force F_b' to remain constant at the force F_p', in the study F_b' is considered equal to F_p' for simplification (Eq. 14) (Fig. 9a).

$$T_{av}' = \frac{\sum_{u=1}^{N_u} T_u}{N_u} \tag{11}$$

$$F_p' = \frac{\sum_{u=1}^{N_u} F_{pu}}{N_u} = \frac{F_p}{N_u} \tag{12}$$

$$T_b' = \frac{\sum_{u=1}^{N_u} T_{bu}}{N_u} \tag{13}$$

$$F'(\delta) = \begin{cases} 0\delta \le \delta_{max} - T_{av}' - 2 \times T_{out} \\ e' \times (\delta - \delta_{max} + T_{av})\delta > \delta_{max} - T_{av}' - 2 \times T_{out} \\ F_p'\delta > \delta_{max} - T_b' - 2 \times T_{out} \end{cases} \tag{14}$$

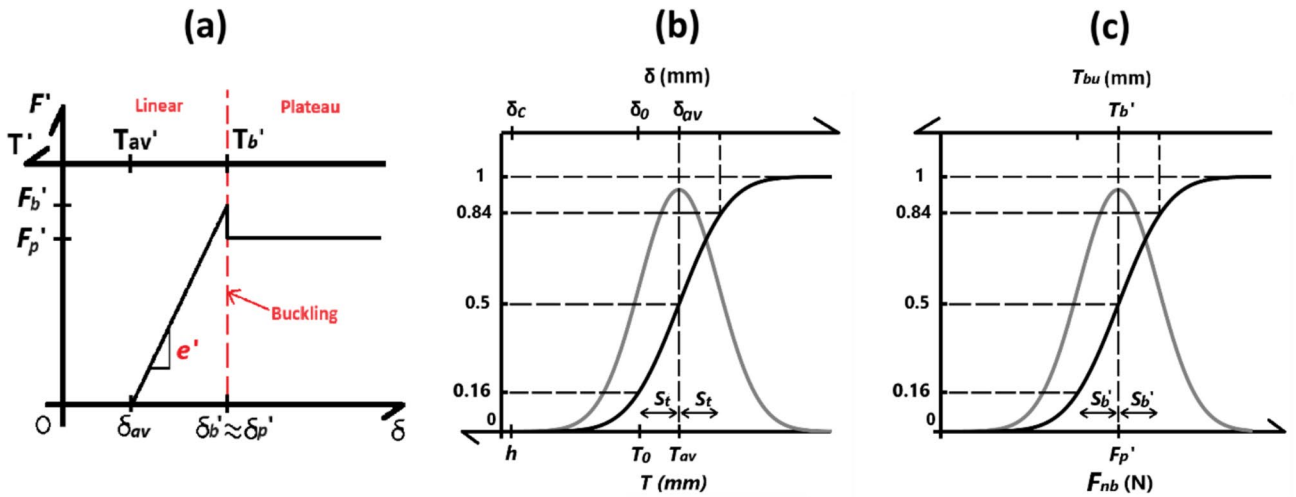

Fig. 9 (**a**) Model compression behaviour of the standard spacer unit. Normal distributions (grey) and its cumulative function (black) of the spacer units (**b**) thickness and (**c**) buckling forces

The distribution of unit thickness follows a normal law of mean T_{av}' and standard deviation S_t. By considering the outer layer thickness T_{out} to be constant, the fabric thickness distribution can be described by a normal law of mean $T_{av}=T_{av}'+2T_{out}$ and standard deviation S_t (Fig. 9b). Its density function f_t and a cumulative function Φ_t are given in function of the compression displacement δ by the Eqs. 15 and 16. The function $\Phi_t(\delta)$ gives the proportion of units having already started their compression at the displacement δ, and Φ_t. Since all the units have the same stiffness e', a compression force F_{nb} neglecting the buckling can be calculated (Eq. 17). F_{nb} is the ideal force of an infinite elastic compression, it needs to be corrected by adding the buckling behaviour to the model.

$$f_t(\delta) = \frac{1}{\sqrt{2\pi {S_t}^2}} e^{-\frac{(\delta-\delta_{av})^2}{2{S_t}^2}} \tag{15}$$

$$\phi_t(\delta) = \int_{-\infty}^{\delta} f_t(x)dx \tag{16}$$

$$\frac{dF_{nb}(\delta)}{d\delta} = \phi_t(\delta) \times N_u \times e' \tag{17}$$

The distribution of unit buckling forces follows a normal law of mean F_p' and standard deviation S_b' (Fig. 9c), its density function f_b' is given in function of the average compression force of a spacer unit F/N_u (Eq. 18). The function Φ_b (F_{nb}) gives the proportion of units having already buckled at the force F_{nb} (Eqs. 19, 20) (Fig. 10c). The buckled units do not participate to the increase of the compression force, it enables the calculation of the compression force of a fabric using the 6 variables: N_u, e', T_{av}', S_t, F_p' and S_b (Eq. 21).

$$f_b'\left(F_{nb}/N_u\right) = \frac{1}{\sqrt{2\pi S_b'^2}} e^{-\frac{\left(F_{nb}/N_u - F_p'\right)^2}{2S_b'^2}} \tag{18}$$

$$f_b(F_{nb}) = \frac{1}{\sqrt{2\pi S_b^2}} e^{-\frac{(F_{nb}-F_p)^2}{2S_b^2}} = 1/N_u \times f_b'\left(F_{nb}/N_u\right) \tag{19}$$

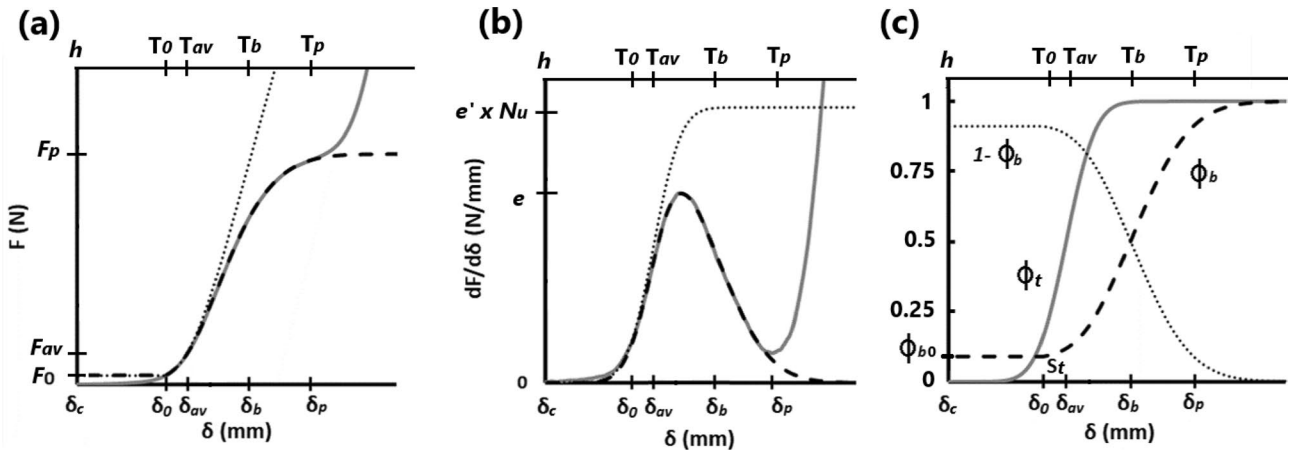

Fig. 10 (**a**) Compression force in function of the displacement of the DA12N5L_1 specimen (grey), its model compression force (long black dots) and its infinite elasticity model compression force F_{nb} (small black dots); (**b**) derivative of the compression force in function of the displacement of the DA12N5L_1 specimen (grey), its model derivative (long black dots) and its infinite elasticity model derivative $dF_{nb}/d\delta$ (small black dots); (**c**) proportion of pressed units (grey), proportion of buckled units (long black dots) and proportion of none buckled units (small black dots)

$$\phi_b(F_{nb}) = \int_{-\infty}^{F_{nb}} f_b(x)dx = \int_{-\infty}^{\frac{F_{nb}}{N_u}} f_b'(x)dx \tag{20}$$

$$\frac{dF(\delta)}{d\delta} = (1 - \phi_b(F_{nb})) \times \frac{dF_{nb}(\delta)}{d\delta} \tag{21}$$

The experimental value of the compression force derivative is calculated with the least squares method (Eq. 22). The experimental force derivative first increases as more units are compressed, after a local maximum is reached the force derivative decreases as more units have buckled until a local minimum before increasing again due to the densification phase. When the derivative reaches the local minimum or becomes negative the compression behaviour enters its plateau phase, the plateau force F_p and plateau thickness T_p of the fabric are measured at this point. The plateau force of the standard unit $F_p' = F_p/N_u$ is then calculated.

$$\frac{\mathrm{d}F}{\mathrm{d}\delta}(\delta_i) = \frac{N \times \sum_{-N/2<j<N/2} F(\delta_{i+j}) \times \delta_{i+j} - \left[\sum_{-N/2<j<N/2} F(\delta_{i+j})\right] \times \left[\sum_{-N/2<j<N/2} \delta_{i+j}\right]}{N \times \sum_{-N/2<j<N/2} (\delta_{i+j})^2 - \left[\sum_{-N/2<j<N/2} \delta_{i+j}\right]^2} \tag{22}$$

The experiment data was processed using a mathematical inverse analysis procedure with a function of the MS-Excel solver [34]. The analysis is a procedure used to determine the fabric average thickness T_{av}, the thickness standard deviation S_t, the unit stiffness e' and the buckling standard deviation S_b. The analysis starts at $\delta_0 = \delta_{av} - S_t$ and finishes at $\delta_p = \delta_{max} - T_p$ when the plateau phase is reached. The analysis cannot start too early because the initial stiffness of the fabric is often caused by its waviness rather than the compression of the thickest spacer units (Fig. 10a, b). The analysis is setting the values of the four variables: the average thickness T_{av}, the thickness standard deviation S_t, the unit stiffness e' and the buckling standard deviation S_b. The parameters $\delta_{\max}$ and N_u are set manually, the parameters δ_0, F_0, δ_{av}, e, T_p, F_p, and T_b are automatically calculated by the Excell sheet. An error coefficient C_s is calculated by summing the square of the difference between the measured and calculated values of $\mathrm{d}F/\mathrm{d}\delta$ (Eq. 23). The analysis sets the optimal combination of variable values for T_{av}, S_t, e' and S_b to reach the minimum value of the error coefficient C_s. After the solver determined the parameters T_{av}, S_t, e' and S_b, the compression force $F(\delta)$ is calculated from δ_0 by adding the integral of the model force derivative between δ_0 and δ to F_0 the force at δ_0 (Eq. 24) (Fig. 10a). The analysis measures the properties of the standard unit: T_{av}', T_b', F_b', F_p' and e'. The variable $T_b = \delta_{max} - \delta_b$ is measured at $F_{nb}(\delta_b) = F_p$ and when half of the units have buckled. The thickness T_{av}' and T_b' are calculated by removing the double of T_{out} to T_{av} and T_b. F_p' is automatically measured before the analysis and e' is directly given by the solver. The standard unit buckling force F_b' is calculated using the Eq. 25 with the measured values of T_{av}', T_b' and e'.

$$C_s(F, \delta_{max}, N_u, T_{av}, e', S_t, S_b) = \sum_{\delta_0<\delta<\delta_p} \left[\frac{dF(\delta)}{d\delta} - (1 - \phi_b(F_{nb})) \times \frac{dF_{nb}(\delta)}{d\delta}\right]^2 \tag{23}$$

$$F(\delta) = F_0 + \int_{\delta_0}^{\delta} (1 - \phi_b(F_{nb}(x))) \times \frac{dF_{nb}(x)}{dx} dx \tag{24}$$

$$F_b' = e' \times (T_{av}' - T_b') = e' \times (T_{av} - T_b) \tag{25}$$

2.4.2 Spacer yarn bending model

During the compression the spacer yarn bends within the plan normal to the warp direction with each half of the yarn bending in an opposite direction. When the yarn finally takes the shape of an S and has its central part almost vertical, it buckles out of the plan. The buckling force of the standard unit can be estimated using the Euler's buckling load formula

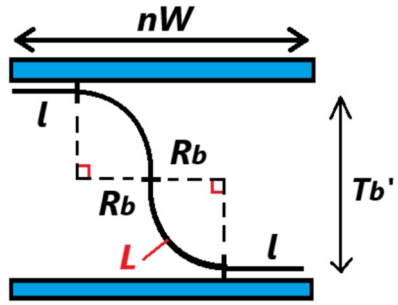

Fig. 11 Geometrical model of the standard unit just before the buckling

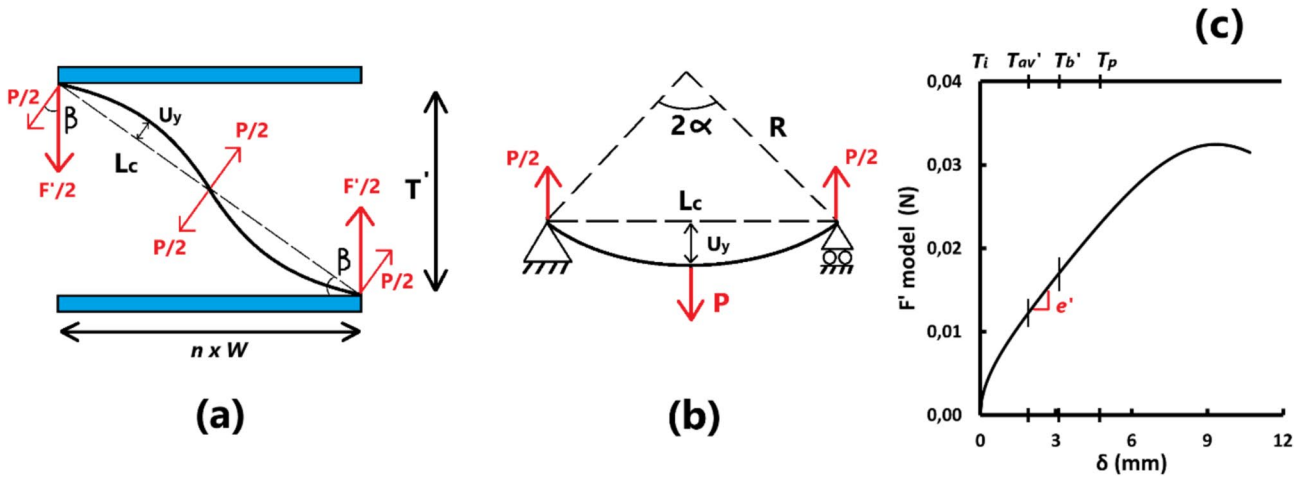

Fig. 12 (**a**) Bending behaviour of the spacer yarn; (**b**) bending behaviour according to the beam theory; (**c**) model bending force of the standard unit of the sample DA12N5

(Eq. 26) with the Young's modulus and the second moment of area *I* (Eq. 27) of the spacer yarn. During the compression the mechanical constraints on the central part of the spacer yarn prevent its extremities to move freely but not to rotate, then the column effective length factor is $K=1$. The only unknown variable of the Eq. 26 is the length L_b of the buckling part of the spacer yarn. The length L_b is equal to T_b' only if the buckling happens when the central part of the yarn is made perfectly straight and vertical before the buckling. By considering that the standard units buckles when it has bent until the spacer yarn took the shape of two equal horizontal lines connected by two equal and opposite arcs, a simple model of the buckling thickness T_b' can be proposed (Eq. 28) (Fig. 11).

$$F_b' = \frac{\pi^2 \times E \times I}{\left(KL_b\right)^2} = \frac{\pi^2 \times E \times I}{{L_b}^2} \tag{26}$$

$$I = \frac{\pi}{4} \times \left(\frac{D_{spacer}}{2}\right)^4 \tag{27}$$

$$T_b' = \frac{L - n \times W}{\pi/2 - 1} \tag{28}$$

On the knitting machine the spacer yarn is straight, but it starts to bend during the shrinkage and continue to do so during the compression test (Eq. 24). By considering that the two halves of the yarn bend as perfect arcs (Eqs. 29–34) (Fig. 12a), the Euler–Bernoulli beam theory can estimate the bending force $P(\delta)$ of each half of the yarn (Eq. 35) (Fig. 12b) and the total compression force $F'(\delta)$ of the standard unit (Eq. 36). The model values of $F'(\delta)$ give the compression behaviour of the standard unit from the shrinkage to the densification phase of the spacer fabric (Fig. 12c). The force $F'(T'=T_{av}')$

gives the compression force applied on the standard unit by the outer layer's contraction. Above the force $F'(T=T_b')$ the standard unit buckles and the behaviour model is not relevant anymore, the compression stiffness e' of the standard unit is then estimated between T_{av}' and T_b' (Eq. 37).

$$T'(\delta) = T_i - \delta \tag{29}$$

$$L_c(\delta) = \frac{1}{2}\sqrt{T'(\delta)^2 + n^2W^2} \tag{30}$$

$$\cos\beta(\delta) = \frac{nW}{2 \times L_c(\delta)} \tag{31}$$

$$\alpha(\delta) = \sqrt{10 - 2\sqrt{60\frac{L_c(\delta)}{L} - 5}} \tag{32}$$

$$R(\delta) = \frac{L}{4 \times \alpha(\delta)} \tag{33}$$

$$U_y(\delta) = R(\delta) - R(\delta) \times \cos\alpha(\delta) \tag{34}$$

$$P(\delta) = \frac{48 \times E \times I \times U_y(\delta)}{L_c(\delta)^3} \tag{35}$$

$$F'(\delta) = \frac{2 \times P(\delta)}{\cos\beta(\delta)} \tag{36}$$

$$e' = \frac{F'\left(T = T_b'\right) - F'\left(T = T_{av}'\right)}{T_{av}' - T_b'} \tag{37}$$

The thickness distribution following a normal law, only 0.13% of the spacer units have a thickness higher than $T_{av}' + 3S_t$, this thickness is considered to be T_i the maximum potential thickness of the units. By starting the compression model at $T=T_i$ (Eq. 29) it can be set that $\delta_{av}=3S_t$ and $T_{av}'=T_i-3S_t$, this prediction of T_{av} gives a simplified expression of Φ_t (Eq. 38). The value of S_b' is strongly dependant of the value of F_b', it is more relevant to use the buckling irregularity $I_b=S_b'/F_b'=S_b/F_b$. Because S_t, and I_b represent the irregularity of the fabric their values cannot be predicted, the average experimental values are used. After introducing I_b and the Euler's buckling load formula (Eq. 26) into the Eq. 20, a simplified expression of Φ_b is given by the Eq. 39.

$$\phi_t(\delta) = \int_{-\infty}^{\delta} \frac{1}{\sqrt{2\pi \times {S_t}^2}} e^{-\frac{(t-3\times S_t)^2}{2\times {S_t}^2}} dt \tag{38}$$

$$\phi_b(F) = \int_{-\infty}^{F} \frac{L^2}{\sqrt{2\pi\left(I_b \times 4 \times \pi^2 E \times I\right)^2}} e^{-\left(\frac{t\times L^2}{\pi^2 E\times I}-1\right)^2 \times \frac{1}{2\times {I_b}^2}} dt \tag{39}$$

Those variables predictions and formulas (Eqs. 36, 38, 39, 40) can predict the compression behaviour of a spacer fabric from the beginning of the flattening to the end of the plateau phase (Fig. 13a). This model compression force was calculated for each sample before being compared to the experimental compression forces of its 3 specimens using an error coefficient C_{mod} (Eq. 41). The model compression starts at $\delta=0$ mm for simplification but it is not the case during

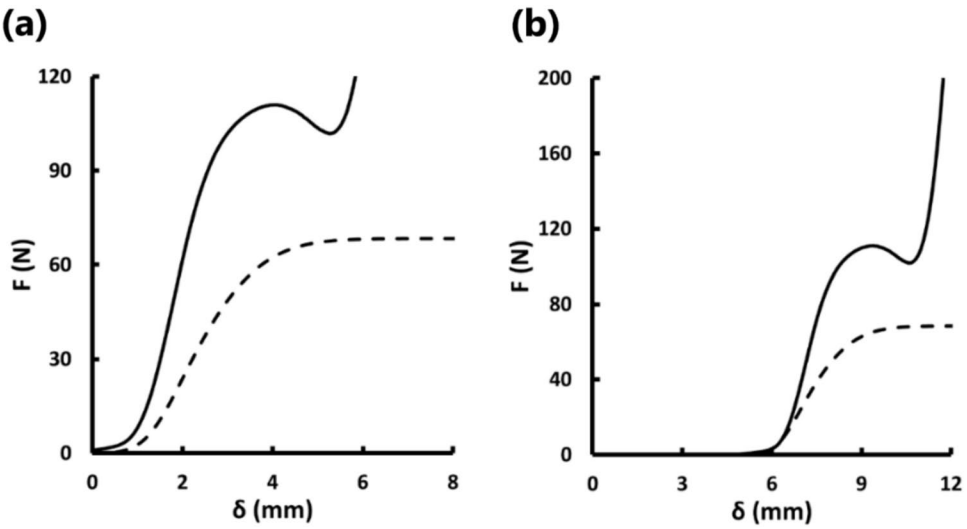

Fig. 13 Experimental (line) and model (dots) values of the spacer fabric compression force in function of the platen displacement (**a**) by considering that the experimental compression starts at $\delta = \delta_{av} - 3S_t$ and (**b**) by predicting the fabric thickness

the experiment, the experimental compression is considered to start at the experimental displacement $\delta = \delta_{av} - 3S_t$. The value $3S_t$ is then removed to the experimental displacement data to make the experimental and model compressions start together. On the opposite the model values can also be adapted to makes a prediction of the compression behaviour including the fabric thickness (Fig. 13b). The model displacement does not start at $\delta = 0$ anymore but at $\delta = \delta_{max} - T_i - 2 \times T_{out}$ (Eq. 42).

$$\frac{dF_{nb}(\delta)}{d\delta} = \phi_t(\delta) \times N_u \times \frac{dF'(\delta)}{d\delta} \tag{40}$$

$$C_{mod} = \frac{average\left|F_{exp}(\delta) - F_{model}(\delta)\right|_{0<\delta<\delta_p}}{average\left(F_{exp}(\delta)\right)_{0<\delta<\delta_p}} = \frac{\int_{\delta=0}^{\delta_p} \left|F_{exp} - F_{model}\right| d\delta}{\int_{\delta=0}^{\delta_p} F_{exp} d\delta} \tag{41}$$

$$\phi_t(\delta) = \int_{-\infty}^{\delta-(\delta_{max}-T_i-2\times T_{out})} \frac{1}{\sqrt{2\pi \times {S_t}^2}} e^{-\frac{(t-3\times S_t)^2}{2\times {S_t}^2}} dt \tag{42}$$

2.5 Method

The specimens were pressed uncut by a circular compression platen of 116 mm diameter with $\delta_{max} = 16$ mm on a benchtop universal testing machine of the grade "EZ-S 500N" (Shimadzu Corporation; Kyoto, Japan) following the protocol reported in the flattening study [31].

3 Results and discussion

3.1 Outer layer properties

The loop height H and loop width W show average experimental values of 1.38 ± 0.11 mm and 1.86 ± 0.16 mm for model values of 1.32 mm and 1.52 mm (Fig. 14a–d). The Pierce model predicts a loop area of 2.01mm^2, which is 21.6% lower than the experimental $A_{loop} = 2.56 \pm 0.33$ mm^2, the W values used for the simulation models can be considered suitable. Despite not including the T_{out}, the ideal thickness T_i matches well the average thickness, showing on average

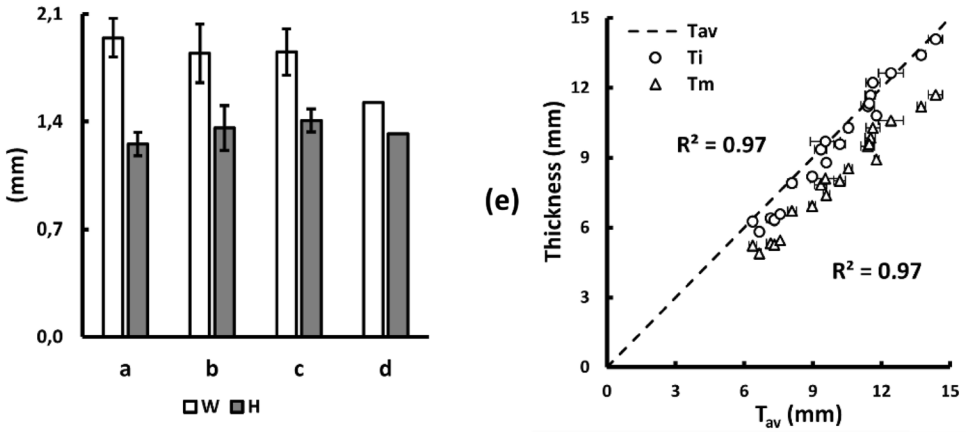

Fig. 14 Average loop width *W* and loop height *H* of the fabric knitted with (**a**) the cotton-acrylic yarn and larger elastic, (**b**) the PET yarn and larger elastic, (**c**) the PET yarn and thinner elastic and (**d**) the prediction model; (**e**) ideal thickness T_i and model thickness T_m of the samples in function of their average thickness T_{av}

only a 5.2% variation from T_{av} (Fig. 14e). This indicates that after the shrinkage the spacer yarn bends a little, the lost thickness is balanced by the thickness T_{out}. The model thickness T_m shows a very high corelation with T_{av} ($R^2 = 0.97$) while always remaining lower than T_{av} due to the outer layer thickness $T_{out} = (T_{av} - T_m)/2$. The difference between T_{av} and T_m is stable as the outer layer's thickness is regular, it tends to show that T_m estimates well the spacer layer's thickness .

3.2 Efficiency of the invert analysis

The models generated by the invert analysis matched the experimental data of the compression force and its derivative very accurately, showing respective average coefficient R^2 of 0.9740 and 0.9997. The dropping of the compression force during the buckling cannot be measured by the compression behaviour model because it considers that $F_p = F_b$. Subsequently the invert analysis systematically provides a value of F_b extremely close to F_p , the later is simply measured with F_p and N_u without using the analysis; F_p shows on average only 2.4% variation from F_b.

3.3 Simulation results

3.3.1 Simulation results of the different geometrical models

The compression force of all the direct models and S-shape models increases sharply at the beginning of the compression to reach its plateau phase extremely quickly and then slowly decreases afterward (Fig. 15a–d). Surprisingly, the straight models and S-shape models both buckles within the plan normal to the warp direction at the beginning of the simulation (Fig. 16a–f). The curved models reach a plateau phase a bit more slowly, without any buckling (Figs. 15e, f, 16g, h).

The straight full arc model follows an almost linear compression behaviour until it buckles and starts its plateau behaviour (Fig. 15g). This simulation result matches the model compression behaviour model of the standard spacer unit and provides precise values for F_b', F_p' and T_b' (Fig. 9a). This model also shows a deformation behaviours close to the experimental behaviour: the yarn bends within the plan to take the shape of a Z, when the central part is almost vertical the yarn bends out of the plan. (Fig. 16i–k). The straight half model keeps bending within the plan without buckling; despite showing an accurate prediction during the linear compression phase it never enters a plateau phase (Fig. 15g). The bend models present results close to the straight full model without showing any buckling, they gradually enter a plateau phase (Fig. 15h). Those models are less interesting than the straight full model for two reasons: they require to set an arbitrary initial bending angle Θ and they do not indicate clearly F_b', F_p' and T_b' like the straight full model does. Some simulations show instability (Fig. 15a, c, e, f) or even stopped before their programmed ends (Fig. 15c, d, h) due to convergence errors, those errors are mainly caused by the limited surface area of the simulation

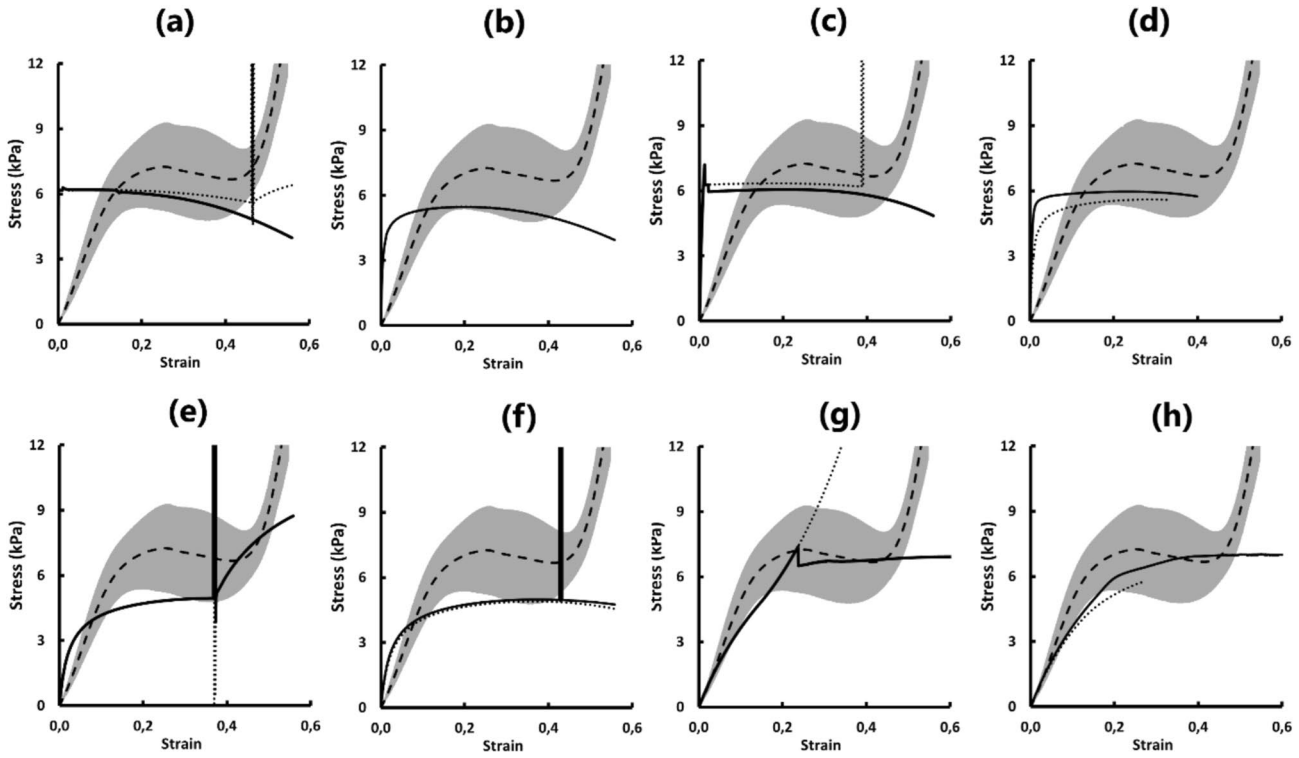

Fig. 15 Stress–strain curves of the average experimental values of the sample A12N5 (long black dots, grey error bars) with the simulation values of the straight models (full: line, half: dots) (**a**) direct, (**c**) S-shaped, (**e**) curved, (**g**) arc and the simulation values of the bent models (Θ = 1°: line, Θ = 5°: dots) (**b**) direct, (**d**) S-shaped, (**f**) curved, (**h**) arc

outer layers. When the spacer yarn bends out of the plan too much, it loses it support from the bottom layer and becomes unstable (Fig. 17). Those errors do not affect the results as they always occur during the plateau phase.

3.3.2 Simulation results of the full straight arc model

For all the simulations using the full straight arc model the force–displacement curves show until the buckling a linear behaviour of average linear coefficient of determination $R^2 = 0.993 \pm 0.001$ (Fig. 18). An error coefficient C_{sim} is calculated until the strain $\varepsilon = 0.4$ to measure the variation of the simulation stress–strain curve from the experimental one (Eq. 43), it shows an average value of $49.6 \pm 38.5\%$.

$$C_{sim} = average\left|\frac{\sigma_{exp}(\varepsilon) - \sigma_{sim}(\varepsilon)}{\sigma_{exp}(\varepsilon)}\right|_{0<\varepsilon<0.4} = \frac{1}{0.4} \times \int_0^{0.4} \frac{\left|\sigma_{exp}(\varepsilon) - \sigma_{sim}(\varepsilon)\right|}{\sigma_{exp}(\varepsilon)} d\varepsilon \tag{43}$$

The simulations predict the plateau stress σ_p and the Young's modulus E with a moderate accuracy, showing respectively on average 29.7% and 39.5% variation from the experimental values (Fig. 19a, b). The simulations predict well the plateau strain ε_p with only a 16.6% average variation from the experimental values. The value of ε_p is relatively stable, with an average value of 0.246 ± 0.020 for the simulations and 0.257 ± 0.072 for the experimental samples. The experimental values are higher because they give the strain of the fabric when the last units reach the plateau phase while the simulation values give ε_p for the standard units.

The simulation predicts accurately the buckling thickness of the standard unit T_b', showing on average a 14.3% variation from the experimental value (Fig. 19c). The simulation T_b' values for models of a same n value are extremely stable, showing on average a 0.06 mm standard deviation for a same knitting structure. It is observed that the average value of T_b' for a given needle distance can be well estimated by $L/2$. The simulation results always show a drop of the compression force at the buckling point, the buckling force F_b' dropping on average of $13.2 \pm 6.6\%$ to reach the

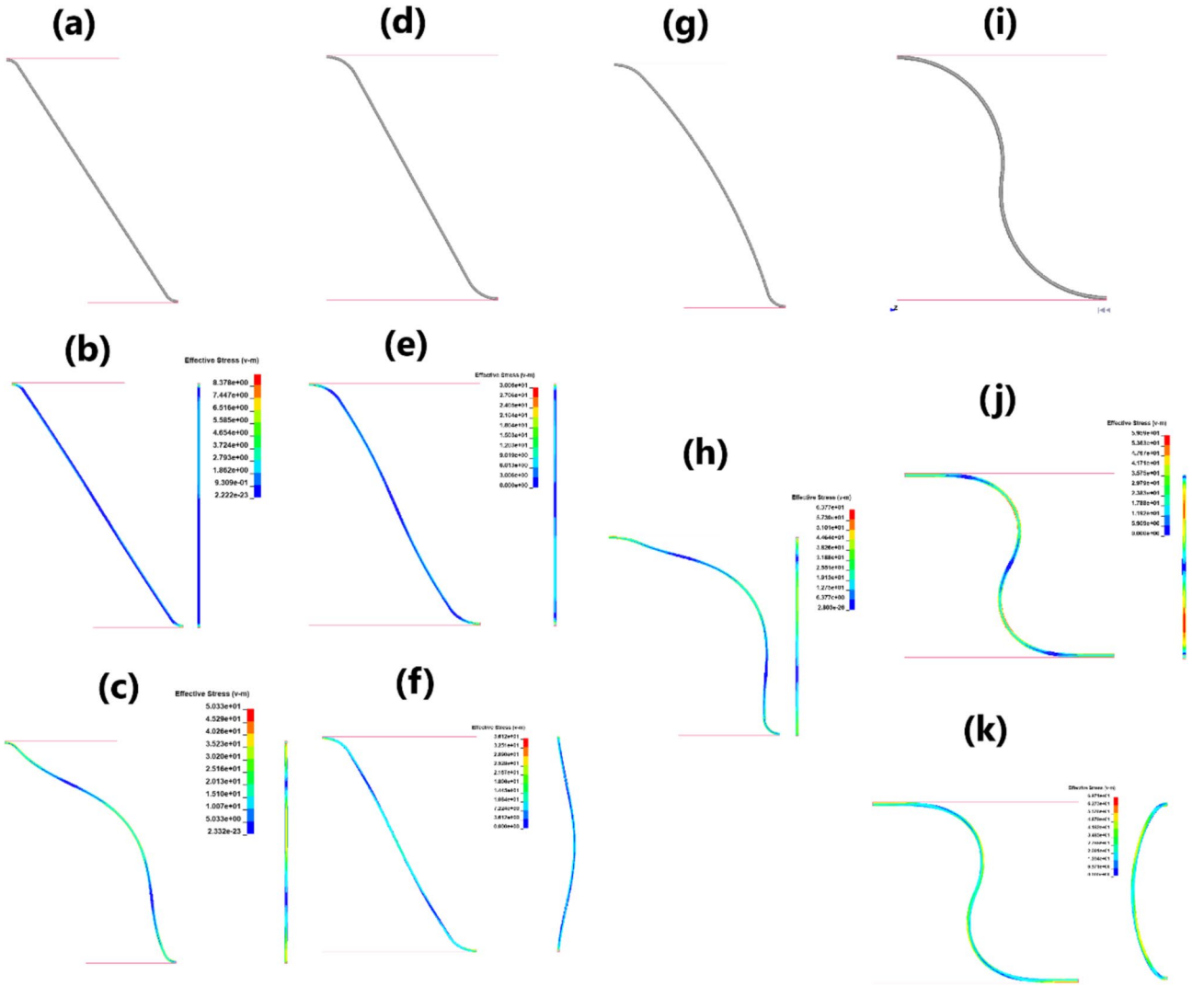

Fig. 16 Simulation straight full models of the direct model (**a**) initial state, (**b**) buckling state, (**c**) at 0.1 strain; of the S-shaped (**d**) initial state, (**e**) buckling state, (**f**) second buckling; of the curved model (**g**) initial state, (**h**) at 0.2 strain; of the arc model (**i**) initial state, (**j**) buckling state, (**k**) plateau state

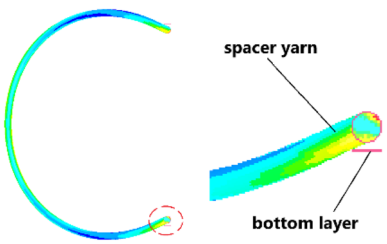

Fig. 17 Weft direction view of an extremely bent simulation spacer yarn leaving the bottom layer

plateau force F_b'. The simulations predict well the buckling F_b' (Fig. 19d) and plateau force F_p' (Fig. 19e) of the standard unit, respectively showing average variations of 26.7% and 28.8% of from the experimental values. The simulation tends to underestimate the spacer unit stiffness e' at the exception of the stiffest samples, showing an average variation of 50.1% from the experimental values (Fig. 19f). Those simulation results lead to the conclusion that the spacer yarn mechanically behaves as two bending opposite arcs, it tends to validate the spacer yarn bending model.

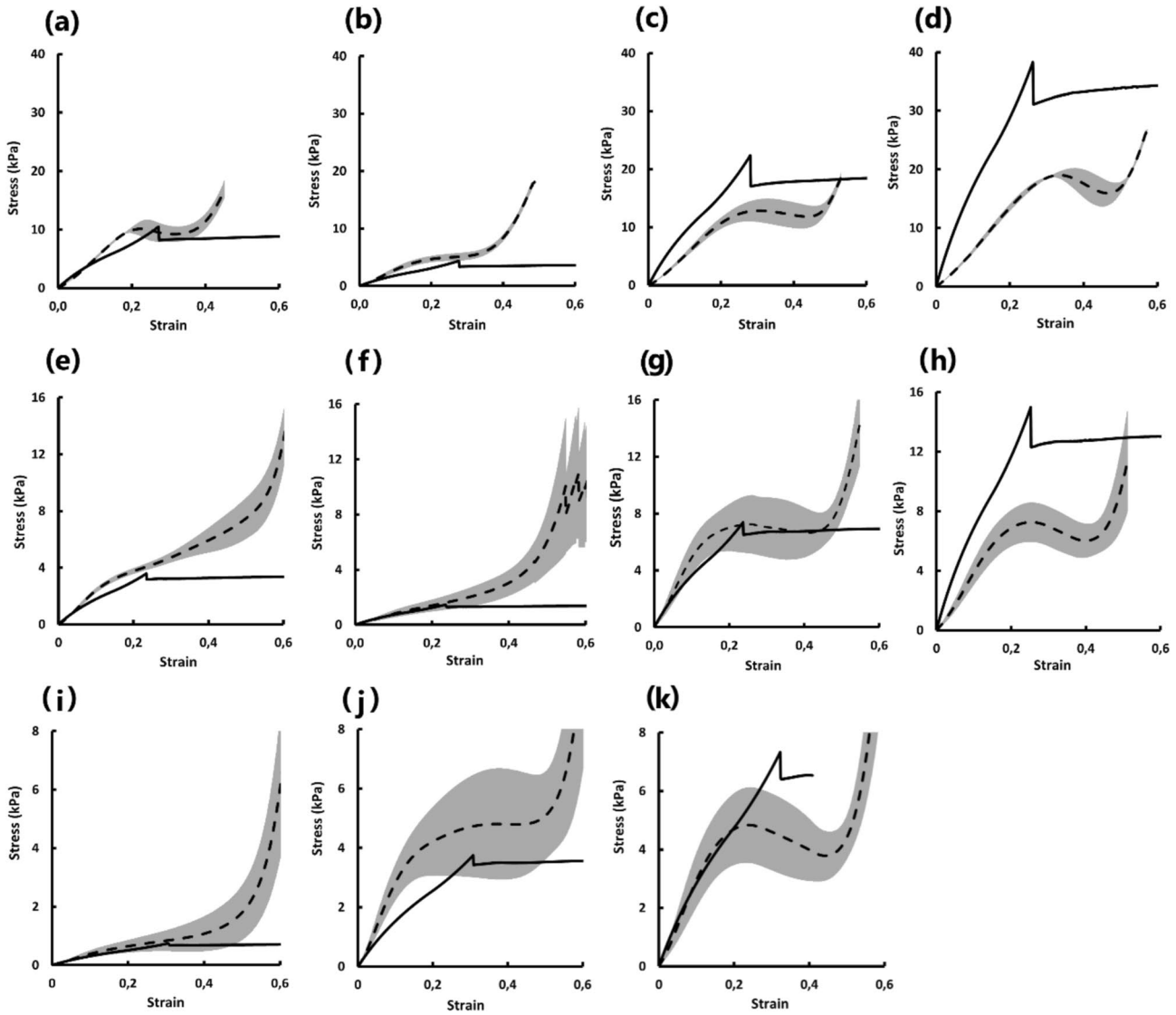

Fig.18 Stress–strain curves of the average experimental values of the samples (long black dots, grey error bars) and simulation values of the straight full arc models (black line) for (**a**) E8N3, (**b**) A8N3, (**c**) A12N3, (**d**) A14N3, (**e**) E8N5, (**f**) A8N5, (**g**) A12N5, (**h**) A14N5, (**i**) A8N7, (**j**) A12N7, (**k**) A14N7

3.4 Mechanical model results

Surprisingly the value of S_t is not correlated at all to the thickness, showing a coefficient of determination $R^2 = 0.019$ with T_{av}. It has an average value of 0.45 ± 0.18 mm which could be linked to the knitting machine geometry or to the shrinkage irregularity. The value of I_b is less stable, showing an average value of 0.55 ± 0.30. Because the analysis prevented the value of I_b to be over 1, the proportion of initially buckled units Φ_{b0} is limited to 16%.

The buckling thickness model predicts relatively accurately T_b', showing on average a 15.9% variation from the experimental value ($R^2 = 0.85$) (Figs. 19c, 20a). The model always overestimates the value of T_b' for the spacer fabrics of needle distance $n = 3$, showing on average a 42.3 ± 4.9% variation from the experimental value for those fabrics. The spacer fabric with lower needle distances n may show a geometry different from the fabrics with higher needle distances.

The Euler's buckling load formula (Eq. 26) predicts the buckling force F_b' of the standard unit with a moderate accuracy if it considers that $L_b = T_b'$. The model values given by the Euler's formula using the experimental (Fig. 20a, b) and model values (Fig. 20c) of T_b' show respective average variation from the experimental F_b' values of 50.9 and 47.2%. This suggests that L_b does not correspond to T_b' and that the central part of the spacer yarn buckles without being vertical. The use of

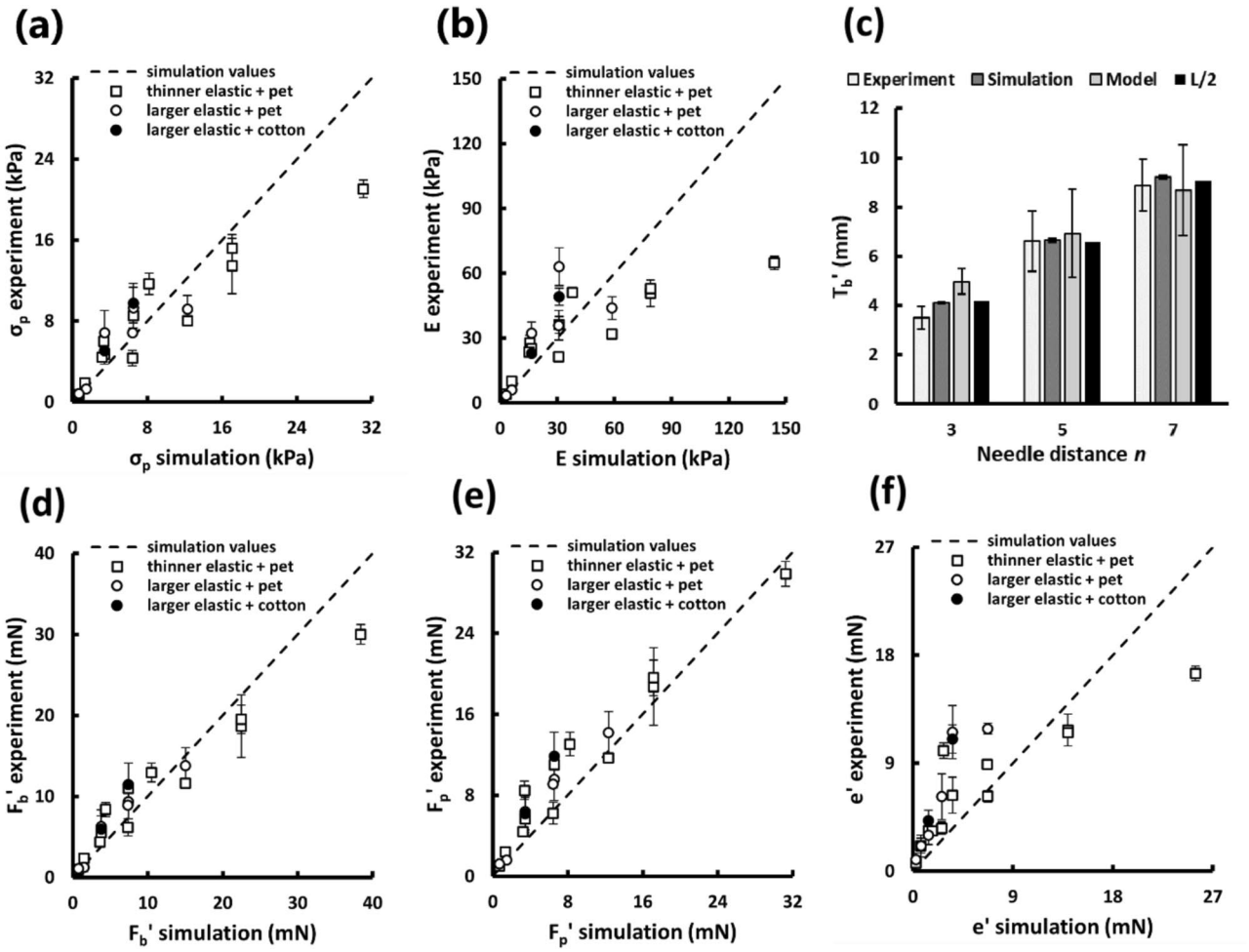

Fig. 19 The experimental values of the (**a**) plateau stress and the (**b**) Young's modulus in function of their simulation values, (**c**) experimental and simulation average values of the buckling thickness T_b in function on the needle distance, (**d**) experimental values of the standard unit buckling force F_b', (**e**) plateau force e_p and (**f**) stiffness e' in function of their simulation values

$L/2$ for the buckling length L_b appears much more efficient, it predicts accurately F_b' with only an average variation from the experimental result of 22.7% (Fig. 20d). This accuracy is evenly distributed to the samples of different needle distance n, it suggests a regularity of the spacer unit's geometry during the buckling. The model value of F_b' calculated with $L_b = L/2$ can be multiplied by the experimental number of unit N_u to obtain a model value of F_p, showing too on average 22.7% variation from the experimental results (Fig. 20e). By knowing n, the diameter and Young's modulus of the spacer yarn and the warp and weft densities of the outer layers, the plateau stress of a weft-knitted spacer fabric can be predicted. The buckling forces calculated using the simulation buckling thickness are extremely close to the buckling forces given by the simulation (Fig. 20f), this indicates that the simulation uses the Euler's formula to simulate the buckling.

The spacer yarn bending behaviour model is very linear until the buckling, the model $F'(\delta)$ shows on average $R^2 = 0.9997$ between T_{av}' and T_b' (Fig. 12c). The model predicts the stiffness e' with a moderate accuracy, showing an average variation of 48.1% from the experimental value (Fig. 20g). The model predicts the value of E (Eq. 44) with a slightly higher accuracy, showing an average variation of 38.7% from the experimental value (Fig. 20h). The invert analysis could have overestimated e' and compensated by underestimating T_{av} to reduce C_s, when calculating E those two errors would balance each other. The model values are again very close to the simulation value, it validates the spacer yarn bending model by showing that *LS-Dyna* uses a very similar model to simulate compression of the arc models (Fig. 20i).

$$E = \frac{e' \times T_{av}}{A_{unit}} \tag{44}$$

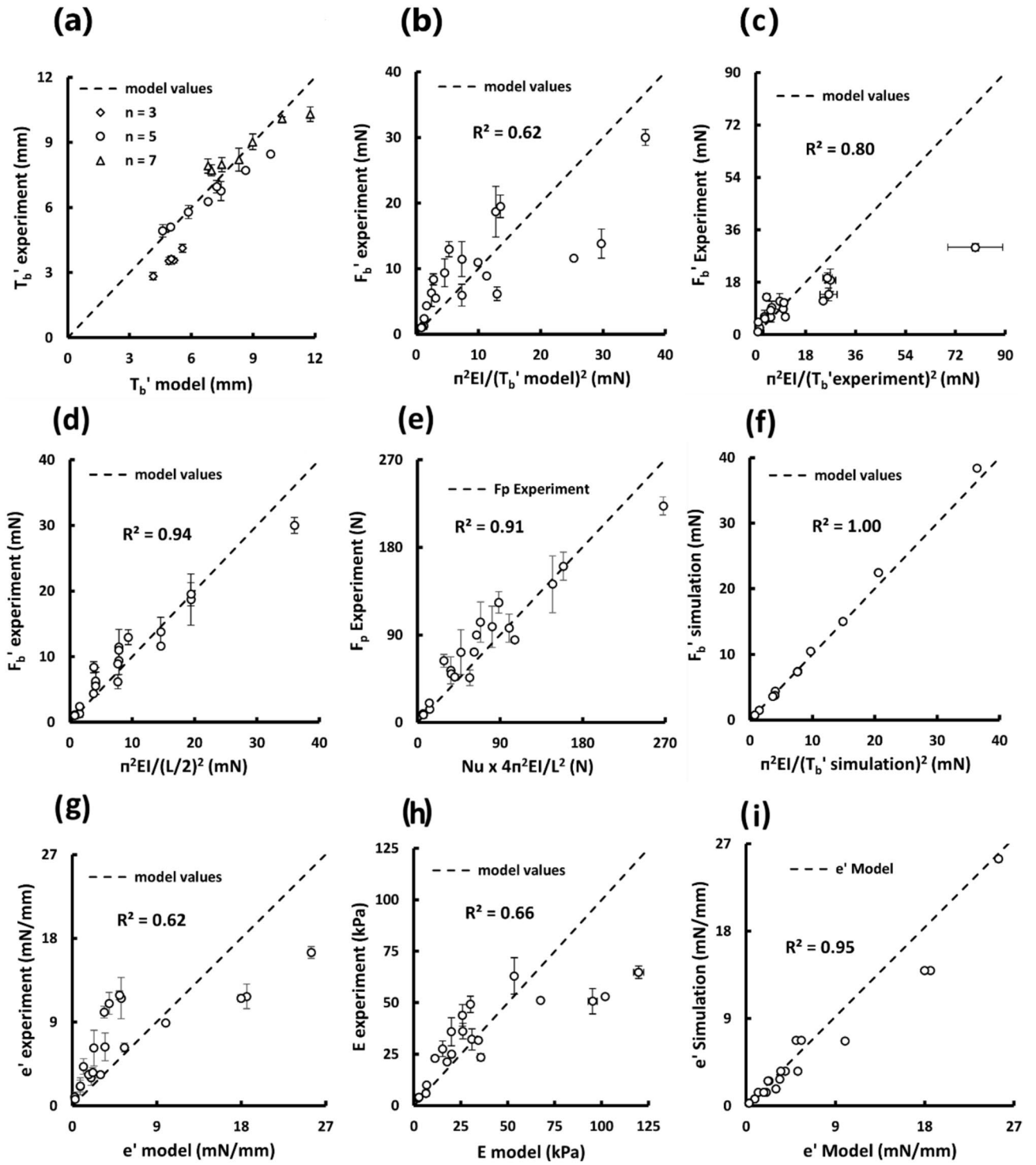

Fig. 20 (**a**) Experimental values of the buckling thickness T_b' in function of the model values; Experimental values of the standard unit buckling force F_b' in function of F_b' calculated using (**b**) the experimental buckling thickness, (**c**) the model buckling thickness and (**d**) half the spacer yarn length; (**e**) Experimental values of the plateau force in function of their model values; (f) Simulation values of standard unit buckling force F_b' in function of F_b' calculated using the simulation buckling thickness; Experimental values of (**g**) the unit stiffness and (**h**) the Young's modulus of the samples in function of their model values; (**i**) Simulation values of the unit stiffness in function of their model values

The hypothesis that $T_{av}' + 3S_t$ matches T_i the maximum potential thickness of the units appears to be correct, the formula $T_{av} + 3S_t - 2T_{out}$ only shows an average variation of 3.4% from T_i. The model can predict the compression behaviour of the sample with a satisfying accuracy by using the average experimental values of S_t and I_b, showing an average error coefficient $C_{mod} = 35.8 \pm 18.2\%$. The specimen DA12N5_1 shows a C_{mod} value of 53.2% (Fig. 13a). The value of C_{mod} doesn't seem to be correlated with any of the fabric's characteristics.

Those results are extremely satisfying, they open the door to easy and quick predictions of weft-knitted spacer fabrics compression behaviour. With a better understanding of the fabric irregularities and a good prediction model for the shrinkage, the compression behaviour could be instantly predicted without even producing any samples nor running a FEA. Solvers could integrate those models to find the exact knitting structure and components to use to knit a spacer fabric with exactly the desired properties. This will be a major economy of time and money for both the academic field and the industry.

4 Conclusion

In this study a total of 20 weft-knitted spacer fabrics with 5 independent parameters was knitted and characterised by a compression test. An invert analysis was conducted with a newly developed compression behaviour model to precisely identify the fabrics average thickness T_{av}, the spacer layers stiffness e', buckling thickness T_b' and buckling forces F_b'. Four simple different geometrical models for the spacer layer were investigated using FEA, the simulation results established that during the compression the spacer yarn behaves like two arcs bending in opposite directions. A second simple geometrical model was developed to describe the geometry of the spacer yarn when it buckles, this model could predict accurately the buckling thickness of the spacer layer T_b' (average error of 15.9%, $R^2 = 0.85$). The Euler's critical load formula was successfully used to predict the buckling force F_b' of the spacer yarn, giving accurate predictions by using half the spacer yarn length as the supported length (average error of 22.7%, $R^2 = 0.94$). By using the Euler–Bernoulli beam theory with the two arcs geometrical model, a linear model ($R^2 = 0.9997$) of the bending behaviour of the spacer yarn can predict with a moderate accuracy the stiffness e' and the Young's modulus E of the spacer fabric (respective average error of 48.1% and 38.7%). By using the spacer fabric compression behaviour model, the spacer yarn bending model and the critical load formula it was possible to predict the fabrics compression force until the plateau phase with only a $35.8 \pm 18.2\%$ average error. These discoveries make possible easy and fast predictions of the mechanical behaviour of the weft-knitted spacer fabrics without going through the production and testing of samples. If the outer layer's densities can be predicted, the presented model can predict the compression behaviour of any weft-knitted spacer fabric using a few simple formulas.

Author contributions U.L. conceptualized the study, processed the data, designed the geometrical models, theorised the compression behaviour model, designed the simulation models, wrote the original draft. U.L and Y.Z. set the simulation conditions Y.Z. runned the simulations U.L. and P.R. made the experimental design, produced the samples and performed the mechanical tests. A.S. guided the methodology and edited the figures A.S. and A.Y. supervised the study and reviewed the manuscript A.Y. provided the material.

Funding The authors Ulysse Le Coz and Pierre Ringenbach received scholarships for PhD candidates, respectively from the National University Corporation Kyoto Institute of Technology Fund and the Otsuka Toshimi Scholarship Foundation.

Data availability All the necessary data to reproduce the results reported here are provided. Readers can access all the experimental data using the provided link: https://nomad-lab.eu/prod/v1/gui/user/search/entry/id/qTSaewXlzCTk7lAkFKg0aoE119wG.

Declarations

Ethics approval and consent to participate Not applicable.

Competing interests The authors declare no competing interests.

References

1. Albaugh L, McCann J, Yao L, Hudson S. Engineering multifunctional spacer fabrics through machine knitting. Conference on Human Factors in Computing Systems, Yokohama, Japan, 8–13 May 2021; https://doi.org/10.1145/3411764.3445564
2. Buzaite V, Mikucioniene D. Effect of inner layer structures of weft-knitted spacer fabrics on thermal insulation and air permeability. Text Res J. 2022. https://doi.org/10.1177/00405175211021452.
3. Klausmann J, Mutschler T, Holderied P, et al. Thermodynamic qualification of knitted spacer fabrics for use as insulation box insert in the context of refrigerated transport containers in the logistics sector. Commun Dev Assem Text Prod. 2023. https://doi.org/10.2536/cdatp.2023.4.p18-26.
4. Wu Q, Hu J. A novel design for a wearable thermoelectric generator based on 3D fabric structure. Smart Mat Struct. 2017. https://doi.org/10.1088/1361-665X/aa5694.
5. Schmidl G, Jia G, Gawlik A, et al. Aluminum-doped zinc oxide–coated 3D spacer fabrics with electroless plated copper contacts for textile thermoelectric generators. Mat Today Energy. 2021. https://doi.org/10.1016/j.mtener.2021.100811.
6. Zheng Y, Zhang Q, Jin W, et al. Carbon nanotube yarn based thermoelectric textiles for harvesting thermal energy and powering electronics. J Mat Chem A. 2020. https://doi.org/10.1039/c9ta12494b.
7. Wang Z, Ruan Z, et al. Integrating a triboelectric nanogenerator and a zinc-ion battery on a designed flexible 3D spacer fabric. Small Method. 2018. https://doi.org/10.1002/smtd.201800150.
8. Li M, Chen J, Zhong W, et al. Large-area, wearable, self-powered pressure-temperature sensor based on 3D thermoelectric spacer fabric. ACS Sens. 2020. https://doi.org/10.1021/acssensors.0c00870.
9. Liu Y, Hu H. Sound absorption behavior of knitted spacer fabrics. Text Res J. 2010. https://doi.org/10.1177/0040517510373639.
10. Ringenbach P, Yu A, Sakuma A. Digital image correlation for measuring strain concentration and distribution mechanics in holed spacer fabrics for knee brace applications. Int J Mec Mat Des. 2025. https://doi.org/10.1007/s10999-025-09743-x.
11. Liu Y, Hu H, Zhao L, Long H. Compression behaviour of warp-knitted spacer fabrics for cushioning applications. Text Res J. 2012. https://doi.org/10.1177/0040517511416283.
12. Rajan T, Souza L, Ramakrishnan G, Zakriya G. Comfort properties of functional warp-knitted polyester spacer fabrics for shoe insole applications. J Ind Text. 2016. https://doi.org/10.1177/1528083714557056.
13. Chen S, Zhang X, Chen H, Gao X. An experimental study of the compression properties of polyurethane-based warp-knitted spacer fabric composites. Autex Res J. 2017. https://doi.org/10.1515/aut-2016-0010.
14. Zhao T, Long H, Yang T, Liu Y. Cushioning properties of weft-knitted spacer fabrics. Text Res J. 2018. https://doi.org/10.1177/0040517517705630.
15. Li N, Yick K, Yu A, Ning S. Mechanical and thermal behaviours of weft-knitted spacer fabric structure with inlays for insole applications. Polym. 2022. https://doi.org/10.3390/polym14030619.
16. Li N, Yick K, Yu A. Novel weft-knitted spacer structure with silicone tube and foam inlays for cushioning insoles. J Ind Text. 2022. https://doi.org/10.1177/15280837211073359.
17. Yu A, Sukigara S, Masuda A. Investigation of vibration isolation behaviour of spacer fabrics with elastic inlay. J Text Eng. 2020. https://doi.org/10.4188/jte.66.65.
18. Yu A, Sukigara S, Masuda A. Vibration isolation properties of novel spacer fabric with silicone inlay. Polym. 2023. https://doi.org/10.3390/polym15051089.
19. Yu A, Sukigara S. Investigation of materials for palm and dorsal of anti-vibration gloves for thermal comfort. Fash Text. 2023. https://doi.org/10.1186/s40691-023-00340-0.
20. Chen F, Liu Y, Hu H. An experimental study on vibration isolation performance of weft-knitted spacer fabrics. Text Res J. 2016. https://doi.org/10.1177/0040517515622149.
21. Chen F, Hu H. Nonlinear vibration of knitted spacer fabric under harmonic excitation. J Eng Fiber Fabr. 2020. https://doi.org/10.1177/1558925020983561.
22. Frydrysiak M, Pawliczak Z. Vibro-insulation properties for spacer knitted fabric as a comparative study. J Ind Text. 2021. https://doi.org/10.1177/1528083719888677.
23. Asayesh A, Amini M. The effect of fabric structure on the compression behaviour of weft-knitted spacer fabrics for cushioning applications. J Text Inst. 2021. https://doi.org/10.1080/00405000.2020.1829330.
24. Asayesh A, Amini M. Analysis of the compression performance of weft-knitted spacer fabrics for protective applications in view of the surface layer structure. Fiber Polym. 2021. https://doi.org/10.1007/s12221-021-0248-y.
25. Ertekin G, Marmarali A. The compression characteristic of weft knitted spacer fabrics. Tekst Konfekt. 2012;22:340–5.
26. Liu Y, Hu H. Compression property and air permeability of weft-knitted spacer fabrics. J Text Inst. 2011. https://doi.org/10.1080/00405001003771200.
27. Wu Z, Xia F. Finite element simulation analysis of compression damage in X-weft-knitted spacer fabrics. J Eng Fib Fabrics. 2024. https://doi.org/10.1177/15589250241302446.
28. Sheikhzadeh M, Ghane M, Eslamian Z, Pirzadeh E. A modeling study on the lateral compressive behavior of spacer fabrics. J Text Inst. 2010. https://doi.org/10.1080/00405000903268796.

29. Chattopadhyay R, Kumar B, Barik P. Rheological model for compression of spacer fabrics. Fiber Polym. 2015. https://doi.org/10.1007/s12221-015-5277-y.
30. Liu Y, Hu H. Compressive mechanics of warp-knitted spacer fabrics. Part I: a constitutive model. Text Res J. 2016. https://doi.org/10.1177/0040517515580530.
31. Le Coz U, Ringenbach P, Sakuma A, Yu A. Flattening behaviour of weft-knitted spacer fabrics. Disc Mec Eng. 2024. https://doi.org/10.1007/s44245-024-00078-z.
32. Peirce FT. Geometrical principles applicable to the design of functional fabrics. Text Res J. 1947;17(3):123–47.
33. el Mogahzy Y. Understanding the Fiber-to-Yarn Conversion System Part II: Yarn Characteristics. 2005; https://www.semanticscholar.org/paper/Understanding-the-Fiber-to-Yarn-Conversion-System-%3A/579e770b790fd89d2875596668c1fb2d3dace2dc?sort=is-influential
34. Harris DC. Nonlinear least-squares curve fitting with microsoft excel solver. J Chem Educ. 1998. https://doi.org/10.1021/ed075p119.